THE ASTROPHYSICAL JOURNAL, 199:669–679, 1975 August 1

MEASUREMENT OF PRIMARY COSMIC-RAY ELECTRONS AND POSITRONS FROM 4 TO 50 GeV

ANDREW BUFFINGTON, CHARLES D. ORTH, AND GEORGE F. SMOOT
Space Sciences Laboratory and Lawrence Berkeley Laboratory, University of California, Berkeley
Received 1974 December 12

ABSTRACT

We have used a bremsstrahlung-identification technique to measure separate e^- and e^+ spectra in the primary cosmic rays from 4 to 50 GeV. Above our average geomagnetic cutoff of 4.0 GV/c, we find fluxes of $4.4 \pm 0.3\ e^-$ and $0.37 \pm 0.09\ e^+$ m^{-2} sr^{-1} s^{-1}. The e^- events follow a differential power law whose spectral index is 2.8 ± 0.1. Our ratio $e^+/(e^+ + e^-) = 0.08 \pm 0.02$ implies traversal of an equivalent slab thickness of 4.3 ± 1.5 g cm^{-2} of interstellar and source material.

Subject headings: abundances, cosmic ray — cosmic rays — interstellar matter

I. INTRODUCTION

The astrophysical importance of e^+ and e^- flux measurements in the primary cosmic rays has been recognized for many years. This importance arises because $e^\pm$ and nuclear cosmic rays are believed to have different propagation histories as a result of the small $e^\pm$ mass, and somewhat different origins because most e^+ are thought to be secondary. The difference in history should be striking at high energies (>100 GeV), where $e^\pm$ propagation is believed to be dominated by radiative effects (inverse Compton scattering and synchrotron losses).

Since the first observation of primary cosmic-ray $e^\pm$ by Earl (1961) and by Meyer and Vogt (1961), well over a dozen research groups have reported measurements which now span a range from a few MeV to about 1000 GeV. Unfortunately, the uncertainties of solar modulation make interpretation of the data below a few GeV difficult or impossible. Disagreement among the measurements at higher energies also makes definitive astrophysical interpretation difficult (Webber 1973). Separate e^+ measurements do not exist above 5 GeV, except for inferences from the east-west asymmetry in arrival direction (Agrinier *et al.* 1969; Anand, Daniel, and Stephens 1969).

In this paper we present the results of separate e^+ and e^- measurements with a balloon-borne instrument. The $e^\pm$ are identified unambiguously through the presence of accompanying bremsstrahlung radiation while background is suppressed to a negligible level. The energies observed (4–50 GeV) extend e^+ measurements by a decade and are above the range strongly affected by solar modulation. We have already reported preliminary e^+ measurements (Buffington, Orth, and Smoot 1974*a*). Here we present our final measurements of the e^+ and e^- fluxes and spectra.

II. INSTRUMENT

Detailed descriptions of our bremsstrahlung-identification technique, our apparatus, and associated accelerator calibrations appear elsewhere (Buffington *et al.* 1973; Buffington, Orth, and Smoot 1974*b*). Only a brief description is given here. Figure 1 shows a schematic diagram. Table 1 presents a summary of specifications for the instrument.

With our magnetic spectrometer technique, $e^\pm$ events are identified using a combination of selective trigger and characteristic event topology. An incident $e^\pm$ emits bremsstrahlung photons while passing through a thin lead radiator. The spectrometer then separates the $e^\pm$ from its bremsstrahlung photons, and records its trajectory for later momentum and sign of charge determination. Finally, the photons and $e^\pm$ enter a shower detector (a lead-plate spark chamber) where both showers are photographed. The resulting two-shower signature—characteristic only of $e^\pm$—permits a rejection of nearly 10^{-5} against other particles (Buffington *et al.* 1974*b*). All background processes, including strong interactions, multiparticle events, and splash albedo, are rejected by the bremsstrahlung and spectrometer criteria. Initial rejection of incident protons, with minimal loss of $e^\pm$, is accomplished by using a trigger scintillator placed below the shower detector, 3 radiation lengths thick, with a threshold at 10 times minimum ionization.

The bremsstrahlung-identification criteria were essential for e^+, because cosmic ray protons outnumber e^+ by about 1000 to 1. Bremsstrahlung identification was not necessary for e^-, since negatively charged cosmic rays other than e^- are comparatively rare. For e^-, we required merely a negative charge and a shower (without prongs) in the lead-plate spark chamber. Nevertheless, only bremsstrahlung-identified e^- were used in calculating the ratio $e^+/(e^+ + e^-)$ to minimize any possible error contribution from uncertainties in the determination of e^+ and e^- efficiencies. These efficiencies were different, corresponding to use of the full bremsstrahlung-identification or merely the e^- shower criteria. Figure 2 shows the expected efficiency curves deduced from calibrations at the Stanford Linear Accelerator Center. The reduced e^+ efficiency with increasing energy was

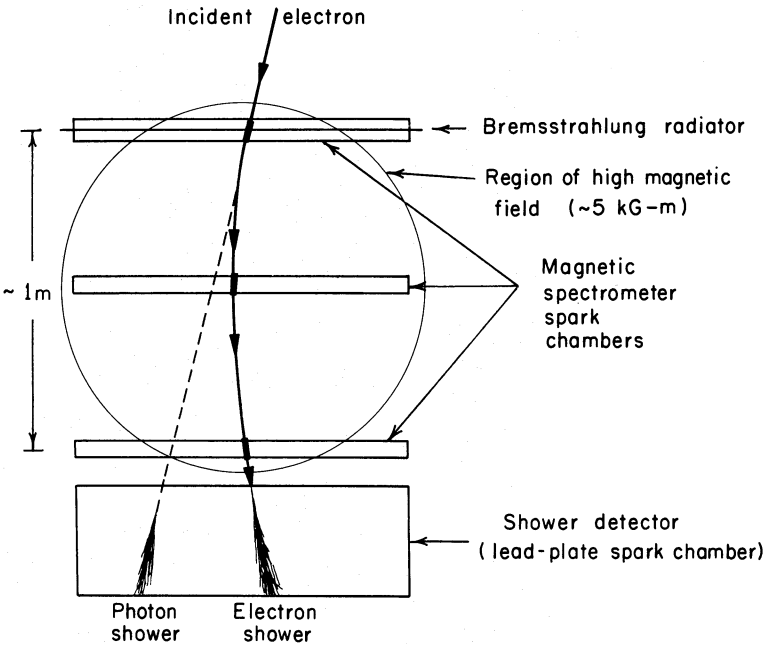

FIG. 1.—Schematic diagram for the apparatus

caused by merging of the bremsstrahlung-photon and e^+ showers.

Two balloon flights were made with this apparatus. For the second flight, we modified the apparatus to achieve a reduction in background trigger rate. This was done by placing an additional 3 radiation lengths of lead below the lead-plate chamber, changing the final trigger counter from Pilot Y scintillator to Pilot 425 Cerenkov radiator, and increasing its threshold to 28 times minimum ionizing. These changes reduced the hadronic interaction background to $\frac{1}{5}$, but reduced the net trigger rate only to $\frac{1}{3}$, since rejection of multiparticle triggers was unaffected. The hadronic background rejection was possible because such interactions have a significant fraction of the outgoing energy in heavy, slow nuclear-spallation fragments. Unfortunately, a leak in the gondola shell caused most of the spark chamber pictures to be of such low quality that we have used flight 2 data merely as a rough cross-check of the results to be reported here from flight 1. For example, the ratio of positively charged to negatively charged $e^{\pm}$ candidates for flight 2 was 24 ± 7 percent, in agreement with the 25 percent observed in flight 1. Table 2 presents flight specifications for the two flights.

III. DATA ANALYSIS

All the data from flight 1 were double-scanned, and nearly half were triple-scanned, for $e^{\pm}$ satisfying the bremsstrahlung-identification criteria. In addition, extra e^- candidates were selected according to the e^- shower criteria. To avoid losing true e^- events, the scanners included some events with small positive curvatures in this extra e^- sample. Cross-checks among the various scans indicated net efficiencies of 99 percent for selecting $e^{\pm}$ which met the bremsstrahlung-identification criteria, and 96 percent for selecting e^- which

TABLE 1

INSTRUMENT SPECIFICATIONS

Geometry factor (m^2 sr)	0.084 ± 0.003
Scattering material within spectrometer	1.4 g cm^{-2}, 0.04 radiation lengths
Spark reconstruction accuracy	0.1 mm per spark chamber (4 gaps)
Resulting specific curvature (charge/momentum) accuracy (1σ for charge $Z = 1$)	$(80\ GV/c)^{-1}$
Bremsstrahlung radiator: lead (aluminum clad)	0.32 radiation lengths
Other gondola material above spectrometer	0.07 radiation lengths
Lead plate spark chamber: 24 gaps:	
6 aluminum plates	0.02 radiation lengths each
19 lead plates	0.16 radiation lengths each
Resulting minimum detectable photon energy	~10 MeV
Incident energy range for bremsstrahlung identification	~1–50 GeV $e^{\pm}$
Camera dead time	0.405 ± 0.002 s per picture

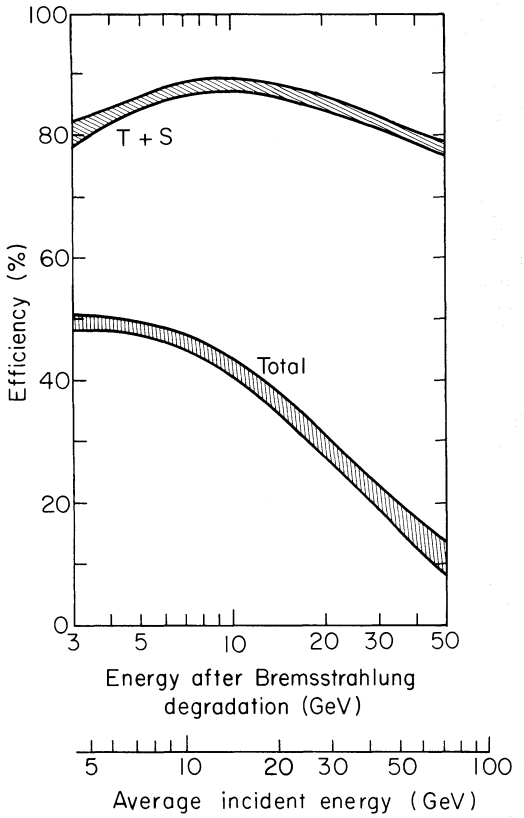

FIG. 2.—Efficiencies for the flight apparatus derived from calibration runs at the Stanford Linear Accelerator Center. *Top curve*, events satisfying both trigger and spectrometer criteria, the proper efficiency curve for e^-. *Bottom curve*, events satisfying the bremsstrahlung-identification criteria, the proper efficiency curve for e^+. The lower energy scale indicates the average incident energy at the top of the atmosphere, for a spectral index of $j = 2.8$.

satisfied *only* the e^- shower criteria. The resulting net e^- scanning efficiency was 98 percent. All selected events were then measured on a manual measuring machine and the measurements analyzed to predict the lead-plate chamber shower locations. Comparison of observed and predicted shower locations removed the last significant non-$e^\pm$ events, leaving no more than than an estimated one or two residual background events (Buffington *et al.* 1974*b*). Table 3 presents the sequence of events passing various stages in the analysis.

Figure 3 presents the distribution of $e^\pm$ events that met all the bremsstrahlung-identification criteria, as a function of measured specific curvature in the gondola. Specific curvature (charge/momentum) is the same as inverse energy for the $e^\pm$ considered here. Figure 4 presents the distribution of the extra e^- events which met only the e^- criteria. The events with positive specific curvature in Figure 4 are presumably high energy proton cosmic rays which had nearly straight trajectories through the momentum spectrometer and showered without prongs in the lead-plate chamber, along with perhaps a few e^+. Monte Carlo calculations indicate that we should expect two of the proton events to "spill over" into the e^- bin immediately to the left of the origin. Correcting for these, we remove the dotted portion of the histogram and obtain the solid histogram in Figure 4 as the proper distribution for true e^- events which were not bremsstrahlung identified. Since the bins of Figures 3 and 4 are about four times wider than our specific curvature resolution, we can neglect any other spillover from bin to bin. In addition, in Figure 3, there are no e^- spilling over into e^+ because the bremsstrahlung photon location uniquely determines sign of charge. (Only one event was reclassified as e^- on the basis of its bremsstrahlung photon location, although its measured specific curvature was slightly positive).

The ratios of the e^- in Figure 4 to those in Figure 3 are in agreement with what we expect from Figure 2. This provides an in-flight cross-check of our efficiency assessment. We have combined all the e^- events from Figures 3 and 4 in making our e^- analysis, and have used the upper curve from Figure 2 for our proper e^- efficiency.

Many of the events of Figures 3 and 4, particularly

TABLE 2

FLIGHT SPECIFICATIONS
(Both balloon flights from Palestine, Texas)

	Flight 1	Flight 2
Date	1972 November 2	1973 May 9
NCAR flight number	720-P	748-P
Float altitude (km)	35.3	35.5
Exposure factor* (m^2 sr s)	165 ± 10	280
Pictures recorded	30,000	15,000
Location at start of data:		
Latitude	32°.2 N	31°.7 N
Longitude	93°.9 W	95°.1 W
Location at end of data:		
Latitude	33°.6 N	31°.0 N
Longitude	88°.1 W	94°.8 W
Geomagnetic cutoff, average from Carmichael *et al.* (1969)	4.0 GV/*c*	4.5 GV/*c*

* The error in exposure factor comes ¾ from camera dead-time uncertainty and ¼ from geometry factor uncertainty.

TABLE 3

ANALYSIS STATISTICS (Flight 1 only)

Events photographed	29261
Events selected as $e^{\pm}$ candidates	1239
Events identified as $e^{\pm}$ by bremsstrahlung	530
Extra events identified as e^{-} by shower and curvature alone	282

those with low momentum, are not primary cosmic rays, but instead are a background of locally produced $e^{\pm}$ due to interactions of other cosmic rays in the residual atmosphere above the apparatus. In another article (Orth and Buffington 1975) we present a detailed analysis and calculation of the expected atmospheric secondaries, as well as an analysis for $e^{\pm}$ produced by similar processes in interstellar space. Here we merely quote the results of these calculations, which are the smooth dashed curves in Figures 3 and 4. The atmospheric background calculations are based on the known interaction properties and flux of protons and do not contain any additional normalization factors. The resulting absolute scale of predicted secondaries could be in error by 20 percent principally because of the 10 percent uncertainty in the flux of primary protons in the 100 GeV range and a 15 percent uncertainty in the dynamical parameters describing proton interactions. Our fit to the events below geomagnetic cutoff (|specific curvature| > 0.25) does not help reduce the uncertainty at high energies because we have utilized the expected 10 percent uncertainty in setting the final trigger scintillator threshold to obtain the fit indicated. This threshold affects only those specific curvatures greater than 1.0 c/GV. The 20 percent uncertainty at high energies is not significant, however, because the background at high energies is quite small. In our calculations, low-energy contributions from re-entrant $e^{\pm}$ albedo have not been included because our data show neither excess of low-momentum events nor anisotropy in arrival direction at low energies.

For cosmic ray data which follow a power-law representation

$$\frac{dN}{dE} = AE^{-j}, \tag{1}$$

bremsstrahlung energy degradation from E to E' merely causes an alteration in the normalization factor A while leaving the spectral index j unchanged (Buffington *et al.* 1974*b*). The degraded spectrum can in fact be represented approximately by

$$\frac{dN}{dE'} = A(j^{-\Delta X/\ln 2})(E')^{-j}, \tag{2}$$

where ΔX is the total thickness in radiation lengths of the material traversed (0.54 for our apparatus, including both atmosphere and gondola). Integral spectral scale similarly under bremsstrahlung degradation. With such scaling, we could in principle determine our measured value of j directly from the differential spectra data measured in the gondola, provided we restricted ourselves to measured values of energy greater than the energy (5 GeV) where geomagnetic-cutoff effects modify the power-law nature of the incident spectrum. Unfortunately, many of our events are lost through bremsstrahlung degradation to energies below cutoff. These lost events are useful, how-

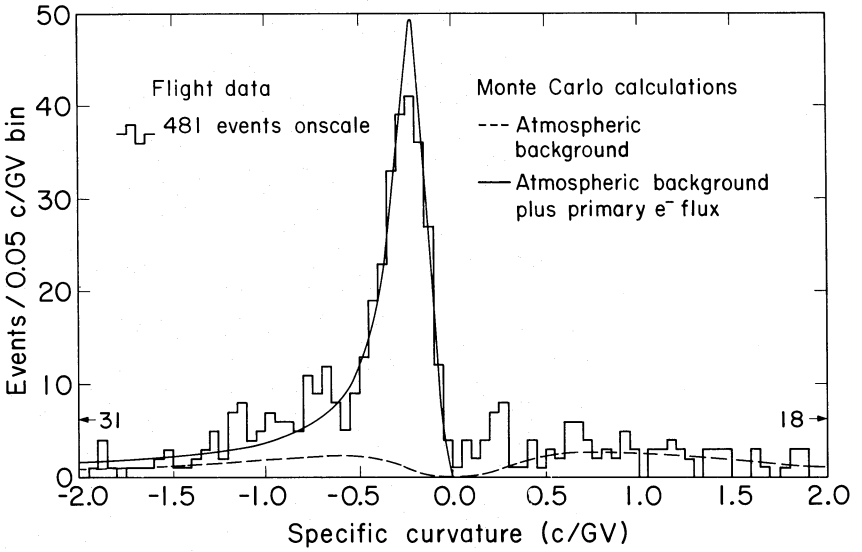

FIG. 3.—Specific curvature (inverse momentum per unit charge) distribution for events meeting all bremsstrahlung criteria

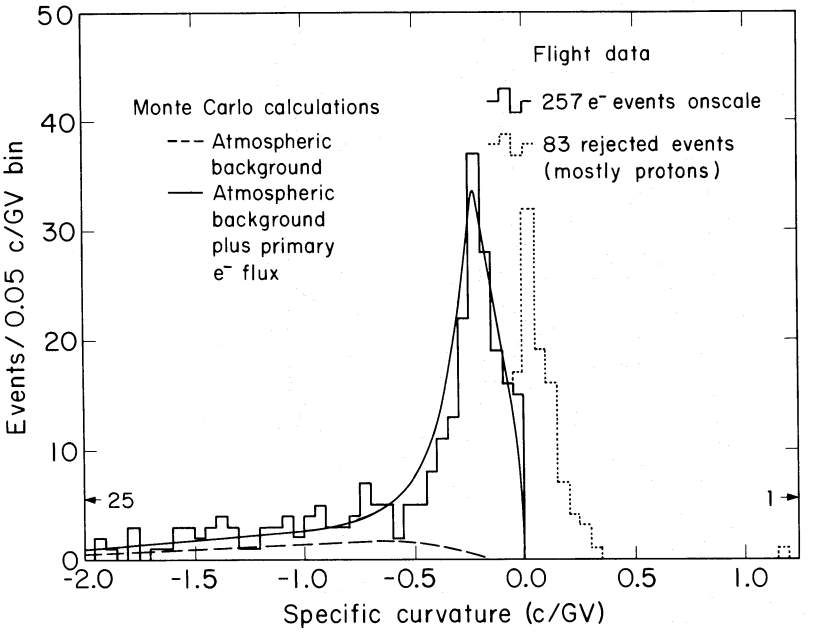

FIG. 4.—Specific curvature distribution for e^- events not meeting the full bremsstrahlung-identification criteria. The dotted histogram shows the events with positive charge; most of the events in the dotted peak cluster to the right in this bin, away from the e^-. Two events were nevertheless able to spill over to the e^- side, according to Monte Carlo calculations.

ever, because the total number of $e^\pm$ events above background represents the integral flux above the average geomagnetic cutoff for our flight.

To get incident energy at the top of the atmosphere, we must invert specific curvature and then scale up by a factor which accounts for the bremsstrahlung degradation in the radiator and overlying atmosphere. This factor is energy and spectrum dependent. For that portion of our data whose measured energy is greater than about 5 GeV, the factor is independent of energy and is $[(j-1)/j]^{-\Delta X/\ln 2} = 1.4$, where $j = 2.8$ is the spectral index and $\Delta X = 0.54$ is the fraction of a radiation length traversed (Buffington *et al.* 1974*b*). Below 5 GeV, geomagnetic-cutoff modifications of the power law cause larger scale-up factors.

We deduce an absolute flux of particles above geomagnetic cutoff by merely counting the number of events in Figures 3 and 4 above the calculated atmospheric background, and dividing by the efficiency and the exposure factor. Below 1 GeV the exposure factors for the events of Figures 3 and 4 are somewhat different, but the difference is only 15 percent by 2.0 *c*/GV.

For the measured differential fluxes and the ratio $e^+/(e^+ + e^-)$ as functions of incident energy, we use only the surviving high-energy events above 5 GeV to avoid scaling factors for bin edges and fluxes which depend on energy. For the ratio $e^+/(e^+ + e^-)$, to avoid possible systematic error from the efficiency curves, we use only bremsstrahlung-identified $e^\pm$.

IV. RESULTS

There are 334 ± 20 e^- and 28 ± 7 e^+ events that lie above the atmospheric contribution of Figure 3. Figure 4 yields an additional 231 ± 17 e^- events above the atmospheric contribution. Using our Monte Carlo calculated efficiency of 77 ± 2 percent for e^- and 46 ± 2 percent for e^+ and our exposure factor of 165 ± 10 m^2 sr s, we calculate absolute fluxes of 4.4 ± 0.3 e^- m^{-2} sr^{-1} s^{-1} and 0.37 ± 0.09 e^+ m^{-2} sr^{-1} s^{-1}.

We have already presented preliminary results of our e^+ measurement (Buffington *et al.* 1974*a*). Averaged over all incident energies, our ratio $e^+/(e^+ + e^-) = 0.08 \pm 0.02$. Figure 5 presents the final $e^+/(e^+ + e^-)$ ratios taken from the bins of figure 3 with energy greater than 5 GeV and with energy scaled by a factor of 1.4 to give equivalent energy at the top of the atmosphere. Also shown on Figure 5 are lower-energy measurements of this ratio by other groups, and our calculated expected ratio for 4 g cm^{-2} of interstellar material (Orth and Buffington 1975). The calculated ratio presented here and the one we presented previously (Buffington *et al.* 1974*a*) differ because we now base our calculations on the recently measured pion-production data of Carey *et al.* (1974) for 50 to 400 GeV. The new calculations raise our estimate of the cosmic ray matter traversed from 3.5 ± 1.5 g cm^{-2} to 5.1 ± 1.5 g cm^{-2}. Figure 5 also shows the ratio expected at lower energies recently presented by Cummings, Stone, and Vogt (1973), which is based on analysis of the nonthermal radio data. The gap between the two curves reflects a difference in assumed $(e^+ + e^-)$ flux rather than measured e^+ flux.

Table 4 gives our integral spectrum analysis for the e^- events. We find $j = 2.8 \pm 0.1$. Since many experiments measure combined $(e^+ + e^-)$ spectra, we have also combined our data into this form, although the

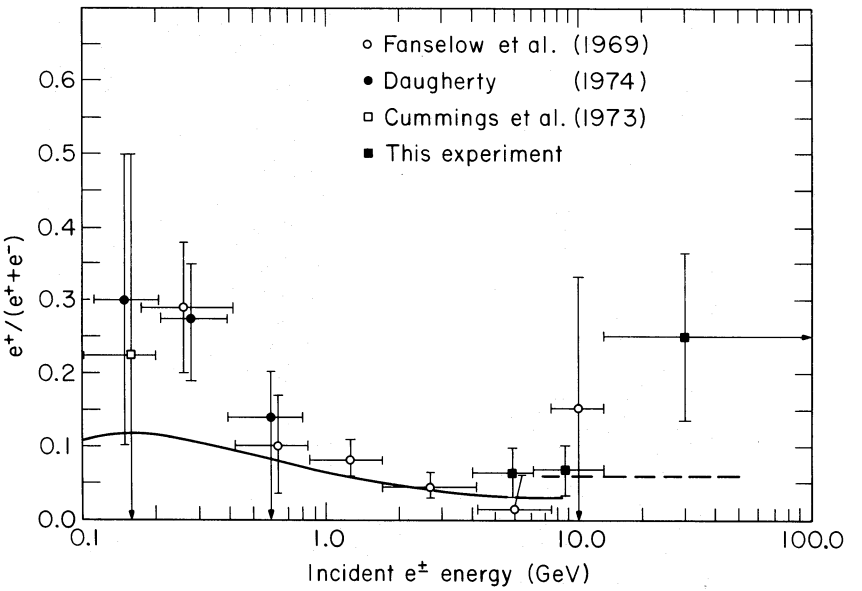

FIG. 5.—Ratio $e^+/(e^+ + e^-)$ as a function of incident energy, corrected to top of atmosphere. Dashed curve indicates the expected level of the ratio of e^+ production from interactions of cosmic ray protons and nuclei with the interstellar gas, divided by our measured $(e^+ + e^-)$ flux (Orth and Buffington 1975). The solid curve at lower energies is the ratio as calculated by Cummings *et al.* (1973) using the nonthermal radio background and the e^+ calculations of Ramaty and Lingenfelter (1968).

analysis is slightly more complicated because of the differing efficiencies for e^+ and e^-. Table 5 presents the analysis for our e^+ and then combined $(e^+ + e^-)$ measurements. Our measured integral fluxes are best fitted by

$$N(>E)_{e^+} = (0.4 \pm 0.1) \times (\tfrac{1}{4}E)^{-1.3\pm0.5} = 2E^{-1.3}, \quad (3)$$

$$N(>E)_{e^-} = (4.4 \pm 0.3) \times (\tfrac{1}{4}E)^{-1.8\pm0.1} = 54E^{-1.8}, \quad (4)$$

$$N(>E)_{e^+ + e^-} = (4.8 \pm 0.3) \times (\tfrac{1}{4}E)^{-1.8\pm0.1} = 59E^{-1.8}. \quad (5)$$

Here we have first expressed energy in terms of ratio to geomagnetic cutoff, in order to uncouple our normalization and spectral index errors.

Most authors present their measurements in terms of differential rather than integral flux measurements. This has the advantage of simple error analysis, since each measured differential point is independent of the others. Table 6 presents our differential flux analysis, for e^-, e^+ and for $(e^+ + e^-)$ data sets. The measured differential fluxes are best fitted by

$$\left.\frac{dN}{dE}\right|_{e^+} = (0.12 \pm 0.03) \times (\tfrac{1}{4}E)^{-2.3\pm0.5} = 3E^{-2.3}, \quad (6)$$

$$\left.\frac{dN}{dE}\right|_{e^-} = (2.0 \pm 0.1) \times (\tfrac{1}{4}E)^{-2.8\pm0.1} = 97E^{-2.8}, \quad (7)$$

TABLE 4

INTEGRAL FLUX ANALYSIS FOR e^-

E' = (specific curvature)$^{-1}$ (GeV)	E: Equivalent Energy above Atmosphere (GeV)*	N_0^-: Observed e^- Events above E'	N_a^-: Calculated e^- Atmospheric Secondaries	Net Events $N_0^- - N_a^-$	e^- Efficiency (from Fig. 2)	Integral e^- Flux $N(>E')$ at Gondola	$N(>E)$ Integral e^- Flux above Atmosphere†
ALL.....	4 (geomagnetic cutoff)	690 ± 26	125 ± 7	565 ± 27	0.77‡	4.45 ± 0.34	4.45 ± 0.34
$E' > 5$.....	7.0	157 ± 13	1.1	156 ± 13	0.82	1.16 ± 0.12	1.39 ± 0.14
$E' > 6.7$....	9.4	93 ± 9.5	0.5	92.5 ± 9.5	0.86	0.66 ± 0.07	0.79 ± 0.08
$E' > 10$.....	14.0	47 ± 7	...	47 ± 7	0.85	0.34 ± 0.05	0.40 ± 0.06
$E' > 20$.....	28.0	19 ± 4.5	...	19 ± 4.5	0.83	0.139 ± 0.031	0.166 ± 0.039

* $E = E'[(j-1)/j]^{-\Delta X/\ln 2} = 1.4E'$ for $j = 2.8$ and $\Delta X = 0.54$.

† $N(>E) = N(>E')(j)^{\Delta X/\ln 2}(E/E')^{1-j} = 1.2N(>E')$ for $j = 2.8$ and $\Delta X = 0.54$.

‡ Monte Carlo result for all events.

1975ApJ...199..669B

TABLE 5

INTEGRAL FLUX ANALYSIS FOR e^+

E' = (specific curvature)$^{-1}$ (GeV)	E: Equivalent Energy above Atmosphere (GeV)	$N_0{}^+$: Observed e^+ Events above E'	$N_a{}^+$ Calculated e^+ Atmospheric Secondaries	Net Events $N_0{}^+ - N_a{}^+$	e^+ Efficiency (from Fig. 2)	Integral e^+ Flux $N(>E')$ at Gondola	$N(>E)$ Integral e^+ Flux above Atmosphere	$N(>E)$ Integral $e^+ + e^-$ Flux above Atmosphere
ALL.....	4 (geomagnetic cutoff)	122	94	28 ± 7	0.46	0.37 ± 0.09	0.37 ± 0.09	4.82 ± 0.35
$E' > 5$.....	7.0	11 ± 3.5	1.5	9.5 ± 3.5	0.42	0.14 ± 0.05	0.16 ± 0.06	1.55 ± 0.15
$E' > 6.7$.....	9.4	7 ± 2.5	0.7	6.3 ± 2.5	0.39	0.10 ± 0.04	0.11 ± 0.05	0.90 ± 0.09
$E' > 10$.....	14.0	5 ± 2.2	...	5 ± 2.2	0.36	0.08 ± 0.04	0.10 ± 0.05	0.50 ± 0.09
$E' > 20$.....	28.0	1 ± 1	...	1 ± 1	0.28	0.02 ± 0.02	0.025 ± 0.025	0.19 ± 0.05

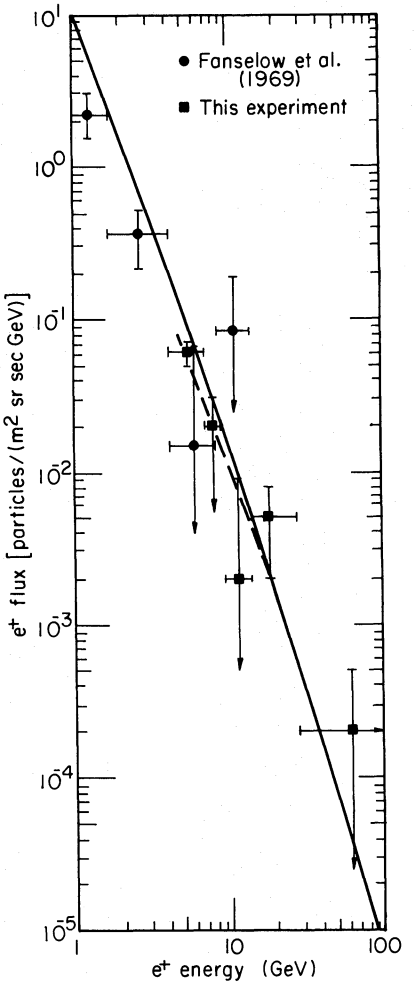

FIG. 6.—Measured e^+ fluxes, and calculated secondary interstellar fluxes (*smooth curves*): ———, Ramaty 1974; – – – –, Orth and Buffington 1975.

$$\left.\frac{dN}{dE}\right|_{e^+ + e^-} = (2.2 \pm 0.1) \times (\tfrac{1}{4}E)^{-2.8 \pm 0.1} = 105E^{-2.8}\,. \qquad (8)$$

In Figure 6 we plot our e^+ flux measurements along with the calculated fluxes of Ramaty (1974) and Orth and Buffington (1975).

V. COMPARISON WITH OTHER $e^+ + e^-$ MEASUREMENTS

Although the e^+ measurements described in the previous section were the primary goal of the experiment, we in addition collected excellent data on the $(e^+ + e^-)$ spectrum. It is not our purpose here to make a critique of other measurements of this spectrum. However, we feel that our powerful rejection of background, detailed identification of $e^\pm$, and detailed efficiency assessment give strong credence to our measurements.

In Figure 7 we present our data points from Table 6, along with other measurements in our energy range. Since Marar, Freier, and Waddington (1971) give only the integral results of their measurement, we generated differential points from their table using a technique similar to that in our Table 6. Although differential plots like Figure 7 are confusing because many points crowd together over many decades, it is nonetheless apparent that many of the experiments disagree by much more than the statistical errors allow.

VI. INTERPRETATION OF RESULTS

Interpretation of our e^+ measurement must be done within the framework of a model for cosmic-ray origin and propagation. Clearly, if some e^+ originate in the sources, our measurement is unable to distinguish between these and others created by interactions of cosmic rays with the interstellar gas. To produce our observed e^+ flux, cosmic-ray protons and heavier nuclei have to traverse 4.3 ± 1.5 g cm^{-2}, which is consistent with the 3–5 g cm^{-2} necessary to produce the observed abundance of Li, Be, and B at low energies. We therefore feel that our measured $e^+/(e^+ + e^-)$ ratio is consistent with no significant e^+ contribution from sources. The bulk of the e^- flux between 1 and 20 GeV, however, must certainly be primary in origin.

Our determination of 4.3 ± 1.5 g cm^{-2} for the mean interstellar path length is based on a simple slab model. An exponential distribution of path lengths would ordinarily be required (Shapiro, Silberberg, and Tsao 1970), but here yields nearly the same answer because the mean path length is less than 10 percent of a proton-interaction mean free path. A simple slab model also ignores diffusive considerations for galactic containment and does not account for the observed change in the L/M ratio between 5 and 50 GeV nucleon^{-1} (see references in Buffington *et al.* 1974*a*). When diffusion is considered, however, essentially the same results are obtained (Orth and Buffington 1975). The only difference is that the 4.3 ± 1.5 g cm^{-2}, rather than describing the mean parent proton path length as one would expect for a slab model, actually describes the mean e^+ path length in interstellar space. We are indebted to R. Ramaty for first pointing this out to us. More recently, the same observation has been made about antiprotons, another species that is presumably only secondary in origin (Gaisser and Levy 1974).

A propagation model consistent with our e^+ data and the L/M observations may be difficult to find. Our measured spectral index $j = 2.8 \pm 0.1$ for e^- is approximately the same as the spectral indices for protons and heavier cosmic rays as measured by Smith *et al.* (1973). We might therefore expect source nuclei, source protons, and source e^- to have similar origins and to experience similar propagation histories within our energy range to the extent that galactic propagation alters their spectra. If such is indeed the case, there may be no viable propagation model which is consistent with 3–5 g cm^{-2} for e^+ in

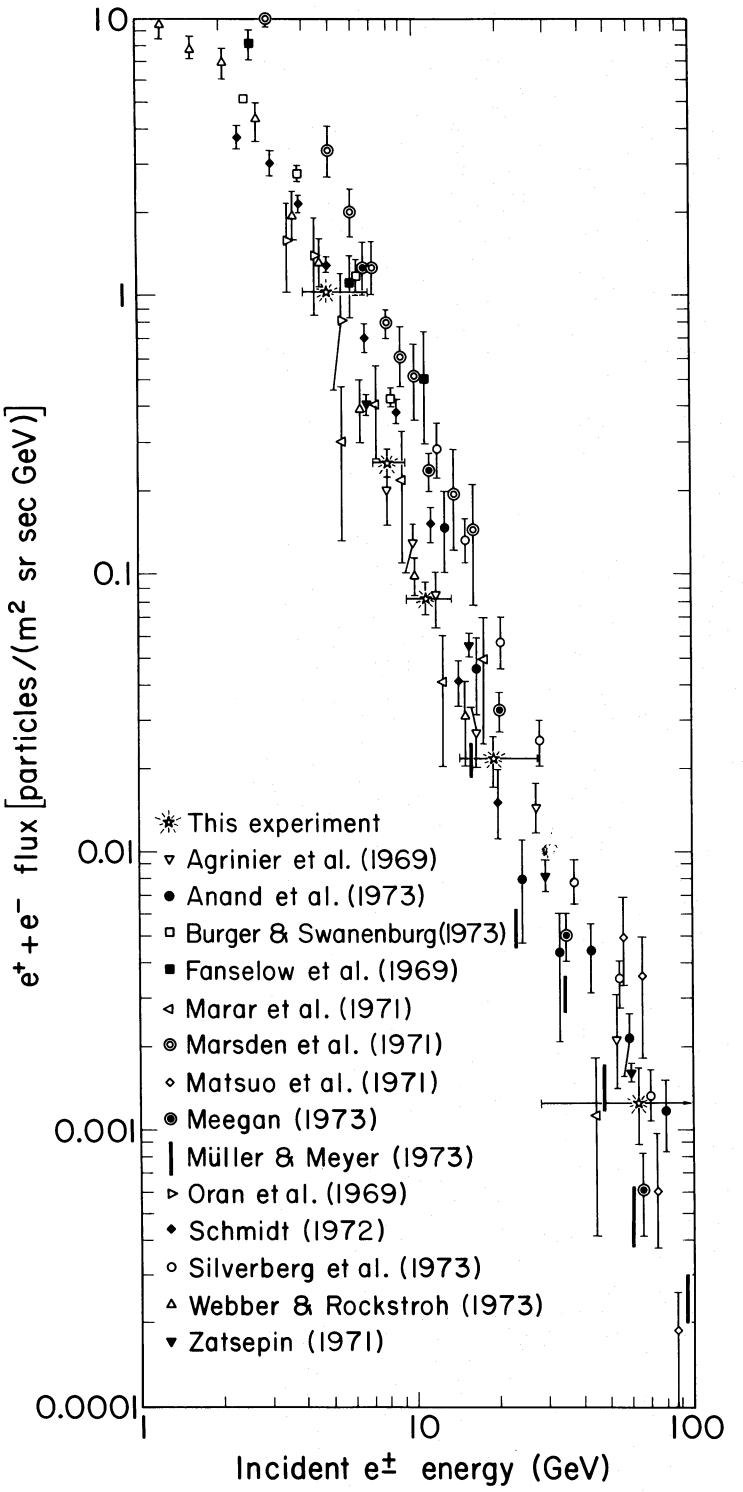

FIG. 7.—Differential $e^+ + e^-$ spectrum as measured in this work, and as measured by various other groups. We have indicated the energy bins only for our data, both to avoid confusion on the plot, and to help distinguish our data from other data.

TABLE 6

DIFFERENTIAL FLUX ANALYSIS (see note added in proof)

E_{min}	E_{max}	$\bar{E}$*	$\Delta E = E_{max}-E_{min}$	$\Delta N = N(>E_{min})-N(>E_{max})$ from Table 4 or 5†	$dN/dE = \Delta N/\Delta E$ (events m^{-2} sr^{-1} s^{-1} GeV^{-1})
			e^-		
4	7	5.1	3	3.06 ± 0.23	1.02 + 0.07
7	9.4	8.0	2.4	0.60 ± 0.08	0.25 → 0.03
9.4	14	11.2	4.6	0.39 ± 0.05	0.085 ± 0.011
14	28	18.8	14	0.23 ± 0.04	0.017 ± 0.003
28	∞	63	‡	0.166 ± 0.034	0.0011 ± 0.0002
			e^+		
4	7	5.1	3	0.20 ± 0.07	0.07 ± 0.02
7	9.4	8.0	2.4	0.05 ± 0.03	0.02 ± 0.01
9.4	14	11.2	4.6	0.02 ± 0.02	0.004 ± 0.004
14	28	18.8	14	0.07 ± 0.04	0.005 ± 0.003
28	∞	63	‡	0.025 ± 0.025	0.0002 ± 0.0002
			$e^+ + e^-$		
4	7	5.1	3	3.26 ± 0.24	1.09 ± 0.08
7	9.4	8.0	2.4	0.65 ± 0.08	0.27 ± 0.03
9.4	14	11.2	4.6	0.40 ± 0.08	0.086 ± 0.013
14	28	18.8	14	0.31 ± 0.07	0.022 ± 0.006
28	∞	63	‡	0.19 ± 0.07	0.0013 ± 0.0004

* $\bar{E} = [(1-j)/(2-j)](E_{max}^{2-j} - E_{min}^{2-j})/(E_{max}^{1-j} - E_{min}^{1-j})$; we have used $j = 2.8$.

† Errors have been computed directly using event statistics rather than the integral flux errors from Tables 4 and 5.

‡ To plot the last integral point as a differential one we divide by a "bin width" of $\Delta E = [(j-2)^{-j}/(j-1)^{1-j}]E_{min} = 5.4E_{min}$ for $j = 2.8$.

the 5–50 GeV range and also consistent with the drop in the L/M ratio in this same range (Orth and Buffington 1975). Perhaps the correct propagation model has yet to be discovered.

We emphasize that our determinations of the expected e^+ flux and a mean interstellar path length of 4 g cm^{-2} is highly dependent on proper knowledge of the absolute flux of protons in the 50–500 GeV range. Although current data are presumably accurate to about 10 percent, these measurements are difficult and have been performed in this energy range and to this accuracy by only two groups. If the proton flux is actually different from what we assume, our e^+ measurements and our estimate of interstellar pathlength will be altered proportionately.

Finally, we note that Badhwar and Golden (1974) have used our $e^+/(e^+ + e^-)$ ratio and recent $\bar{p}$ production data to put a theoretical limit of approximately 10^{-4} on the $\bar{p}/p$ ratio in the cosmic rays.

We are grateful for the fine service and hospitality offered us by the staff of the National Center for Atmospheric Research Balloon Facility at Palestine, Texas. The accelerator calibrations were carried out at the Lawrence Berkeley Laboratory Bevatron and at the Stanford Linear Accelerator Center. We acknowledge useful conversations with R. Cowsik, P. S. Freier, J. F. Ormes, R. Ramaty, S. A. Stephens, W. R. Webber, and L. W. Wilson. We have enjoyed numerous suggestions and support from L. W. Alvarez, P. M. Dauber, R. A. Muller, and L. H. Smith. This work was supported by contract NAS 9-7801 and grant NGR-05-003-553 from the National Aeronautics and Space Administration and by the Lawrence Berkeley Laboratory.

REFERENCES

Agrinier, B., Koechlin, Y., Parlier, B., Paul, J., Vasseur, J., Boella, G., Sironi, G., Russo, A., and Scarsi, L. 1969, *Conference Papers, 11th International Conference on Cosmic Rays*, Budapest, **1**, 203.

Anand, K. C., Daniel, R. R., and Stephens, S. A. 1969, *Conference Papers, 11th International Conference on Cosmic Rays*, Budapest, **1**, 235.

———. 1973, *Conference Papers, 13th International Conference on Cosmic Rays*, Denver, **1**, 355.

Badhwar, G. D., and Golden, R. L. 1974, *Nature*, **251**, 126.

Buffington, A., Orth, C. D., and Smoot, G. F. 1974*a*, *Phys. Rev. Letters*, **38**, 34.

———. 1974*b*, *Nucl. Instr. and Meth.*, **122**, 575.

Buffington, A., Smoot, G. F., Smith, L. H., and Orth, C. D. 1973, *Conference Papers, 13th International Conference on Cosmic Rays*, Denver, **1**, 318.

Burger, J. J., and Swanenburg, B. N. 1973, *Conference Papers, 13th International Conference on Cosmic Rays*, Denver, **5**, 3061.

Carey, D. C., Johnson, J. R., Kammerud, R., Peters, M., Ritchie, D. J., Roberts, A., Sauer, J. R., Shafer, R., Theriot, D., Walker, J. K., and Taylor, F. E. 1974, *Phys. Rev. Letters*, **33**, 327 and 330.

Carmichael, H., Shea, M. A., Smart, D. F., and McCall, J. R. 1968, *Canadian J. Phys.*, **47**, 2067.

Cummings, A. C., Stone, E. C., and Vogt, R. E. 1973, *Con-*

ference Papers, 13th International Conference on Cosmic Rays, Denver, **1**, 340.
Daugherty, J. K. 1974, Goddard Space Flight Report No. X-660-74-16 (to be published).
Earl, J. A. 1961, *Phys. Rev. Letters*, **6**, 125.
Fanselow, J. L., Hartman, R. C., Hildebrand, R. H., and Meyer, P. 1969, *Ap. J.*, **158**, 771.
Gaisser, T. K., and Levy, E. H. 1974, *Phys. Rev. D*, **10**, 1731.
Marar, T. M. K., Freier, P. S., and Waddington, C. J. 1971, *J. Geophys. Res.*, **76**, 1625.
Marsden, P. L., Jakeways, R., and Calder, I. R. 1971, *Conference Papers, 12th International Conference on Cosmic Rays*, Hobart, **1**, 110.
Matsuo, M., Mikumo, E., Nishimura, J., Niu, K., and Taira, T. 1971, *Conference Papers, 12th International Conference on Cosmic Rays*, Hobart, **7**, 2550.
Meegan, C. A., and Earl, J. A. 1974, University of Maryland Technical Report No. 75-019 (to be published).
Meyer, P., and Vogt, R. 1961, *Phys. Rev. Letters*, **6**, 193.
Müller, D., and Meyer, P. 1973, *Ap. J.*, **186**, 841.
Oran, W. A., Frye, G. M. Jr., and Wang, C. P. 1969, *J. Geophys. Res.*, **74**, 53.
Orth, C. D., and Buffington, A. 1975, to be published.
Ramaty, R. 1974, in *High Energy Particles and Quanta in Astrophysics*, ed. F. B. McDonald and C. E. Fichtel (Cambridge: MIT Press), chap. 3.
Ramaty, R., and Lingenfelter, R. E. 1968, *Phys. Rev. Letters*, **20**, 120.
Schmidt, P. J. 1972, *J. Geophys. Res.*, **77**, 3295.
Shapiro, M. M., Silberberg, R., and Tsao, C. H. 1969, *Conference Papers, 11th International Conference on Cosmic Rays*, Budapest, **1**, 471.
Silverberg, R. F., Ormes, J. F., and Balasubrahmanyan, V. K. 1973, *Conference Papers, 13th International Conference on Cosmic Rays*, Denver, **1**, 347.
Smith, L. H., Buffington, A., Smoot, G. F., Alvarez, L. W., and Wahlig, M. A. 1973, *Ap. J.*, **180**, 987.
Webber, W. R. 1973, *Conference Papers, 13th International Conference on Cosmic Rays*, Denver, **5**, 3568.
Webber, W. R., and Rockstroh, J. M. 1973, *J. Geophys. Res.*, **78**, 1.
Zatsepin, V. I. 1971, *Conference Papers, 12th International Conference on Cosmic Rays*, Hobart, **5**, 1720.

Note added in proof. In Table 6 one should really use $\Delta E = \int_{E_{\min}}^{E_{\max}} E^{-1} dE / \bar{E}^{-1}$, but this causes no more than a 10 percent change here. Besides, the fit to these dN/dE derivatives may be inconsistent with equations (6)–(8), since the latter are derivatives of equations (3)–(5). We consider the integral data and fits to be more accurate. Finally, because of the small statistics, we note that an asymmetrical error assignment for our e^+ flux and the implied material traversal would be more correct.

ANDREW BUFFINGTON, CHARLES D. ORTH, and GEORGE F. SMOOT: Room 50-232, Lawrence Berkeley Laboratory, Berkeley, CA 94720